3-D Scattering From a PEC Target Buried Beneath a Dielectric Rough Surface: An Efficient PILE-ACA Algorithm for Solving a Hybrid KA-EFIE Formulation

Sami Bellez, Christophe Bourlier, and Gildas Kubické

Abstract—An efficient hybrid KA-EFIE formulation is deployed to analyze the electromagnetic (EM) scattering from a 3-D perfectly electric conducting (PEC) object buried beneath a 2-D dielectric rough surface. In this approach, the electric and magnetic current densities on the rough surface are analytically obtained through the current-based Kirchhoff approximation (KA), whereas the electric current density on the buried object is rigorously determined by solving the electric field integral equation (EFIE) using the Galerkin's method of moments (MoM) with Rao–Wilton–Glisson (RWG) basis functions. The KA-EFIE matrix system is then efficiently solved by the iterative propagation-inside-layer-expansion (PILE) method combined with the algebraic adaptive cross approximation (ACA). The current densities on the dielectric rough surface are thereafter used to handle the bistatic normalized radar cross-section (NRCS) patterns. The proposed hybrid approach allows a significant reduction in computation time and memory requirements compared to the rigorous Poggio–Miller–Chang–Harrington–Wu (PMCHW)-EFIE formulation which requires solving a large MoM matrix equation. Moreover, the hybridization of the ACA algorithm with the PILE method improves further the computational cost thanks to the rank-deficient propriety of the coupling matrices. To validate the hybrid approach, we compare its results with those of the rigorous PMCHW-EFIE approach.

Index Terms—Adaptive cross approximation (ACA), EM scattering, hybridization, Kirchhoff approximation (KA), propagation-inside-layer-expansion (PILE) method.

I. INTRODUCTION

IN recent years, the characterization of electromagnetic (EM) scattering from a perfectly electric conducting (PEC) object buried beneath a dielectric rough surface has attracted much interest owing to its extensive applications to terrain radar remote sensing and buried target detection. Some rigorous approaches based on solving surface integral equation formulations with a method of moments (MoM) [1]–[3] are investigated for both 2-D [4]–[6] and 3-D [7]–[11] scattering problems. Depending on the surface that encloses the object

(open object or closed object) and its EM parameters (PEC or dielectric), an appropriate choice of an integral formulation can be made. For instance, the electric field integral equation (EFIE) formulation [12] is often used for an open PEC object, whereas the magnetic field integral equation (MFIE) formulation [13] or the combined field integral equation (CFIE) formulation [14], as it eliminates interior resonance problem, are, respectively, applied on the boundary of a closed object. Furthermore, the Poggio–Miller–Chang–Harrington–Wu (PMCHW) formulation [15], [16] is frequently preferred to deal with the scattering from a dielectric homogenous object, as it yields to a better conditioned matrix equation as compared to EFIE and MFIE formulations.

Usually, the rough surface is modeled by a finite-size surface, due to limited computing resources, and a tapered incident beam is simulated in order to circumvent artificial edge diffraction effects, occurring when an incident plane wave illumination is considered. In fact, simulating the incident wave by a tapered Gaussian beam, forces the equivalent current levels on the rough surface to be extremely low away from the footprint center, thereby the finite-length rough surface can be viewed as an infinite (closed) surface separating two homogenous domains. On the other hand, by considering an object beneath the rough surface, the scattering problem becomes more complicated because of multiple scattering interactions between the buried object and the rough surface. Indeed, edge diffraction effects can eventually take place when the field scattered by the buried object greatly illuminates the edges of the truncated rough surface. Therefore, this latter must have electrically large dimensions in an attempt to eliminate the edge diffraction phenomenon. However, this increases both computational time and memory requirements and prevents the direct solving of the MoM matrix equation (arising from the MoM discretization of the PMCHW integral equations). For this reason, computationally efficient methods based on MoM as the sparse-matrix canonical grid (SMCG) method [17]–[19] and the steepest descent fast multipole method (SDFMM) [20] was adopted to overcome this difficulty.

Different from the purely numerical methods, this paper offers a methodology providing a clear merger of an asymptotic technique with an integral equation formulation numerically solved by an MoM-based technique in order to achieve a significant reduction in CPU time and memory requirements. The

basic idea of this work is to apply the asymptotic current-based Kirchhoff approximation (KA) [21], [22], also sometimes referred to as the tangent plane approximation, in order to analytically obtain the electric and magnetic current densities on the dielectric rough surface. This approximation assumes that the current densities at any point on the rough surface are those that would be present on an infinite tangent plane at that particular point. Thus, the current densities are expressed in terms of the field illuminating the surface and the local Fresnel reflection coefficients, as the reflection is assumed to be locally specular. The KA is a very attractive alternative, when applicable (valid for large radius of curvature relative to the incident wavelength at every point on the surface), because it avoids the inversion of the self-impedance matrix of the rough surface arising from an MoM discretization of the PMCHW surface integral equations. Moreover, an integral equation formulation seems to be well-adapted to address the scattering from the PEC-buried object in as much as the involved MoM matrix equation is often of small or moderate size and can be solved efficiently.

Consequently, a powerful hybrid approach considering the rough surface as a KA region and the PEC-buried object as an EFIE region (if needed, the CFIE formulation can also be applied instead of the EFIE formulation) is adopted. The hybrid KA-EFIE formulation is then converted into a matrix equation by using an MoM with RWG basis functions [12] defined on triangular patches discretizing both regions. The resolution is achieved by the iterative propagation-inside-layer-expansion (PILE) method [23] which is suitable for scattering problems involving two scatterers where only one is illuminated by the incident EM wave. The PILE method is based on the partitioned inverse matrix formulas and an iterative scheme in which, for this paper, the algebraic adaptive cross approximation (ACA) [24] is incorporated. The resulting method is named PILE-ACA method. The ACA expresses a matrix $\mathbf{Z}$ as a product of two matrices, typically referred to as $\mathbf{U}$ and $\mathbf{V}$ and it is used to compress the matrices characterizing the interactions between the rough surface and the buried object. This technique is very useful to speed-up the filling of these matrices as well as to accelerate the matrix–vector products. The paper is organized as follows. Section II presents the rigorous PMCHW integral equations-EFIE of the scattering problem and describes the hybridization of the current-based KA with the rigorous EFIE formulation. Section III deals with the MoM discretization procedure and the resolution of the hybrid matrix equation with PILE and PILE-ACA methods. Section IV shows the numerical results of the hybrid KA-EFIE approach compared with those of the rigorous PMCHW-EFIE approach. Finally, Section V gives concluding remarks.

II. RIGOROUS AND HYBRID FORMULATIONS

A. Problem Geometry

Let us consider the scattering of a tapered incident wave ($\overline{\mathbf{E}}_1^{inc}$, $\overline{\mathbf{H}}_1^{inc}$), when assuming the time harmonic dependence $\exp(j\omega t)$, by a 3-D PEC object buried under a 2-D dielectric Gaussian rough surface with a random height profile $z = f(x, y)$. The Braunisch approximate 3-D vector-tapered wave

[25] is employed in this paper since it can be evaluated without resorting to any numerical integrations. The height function $z = f(x, y)$ has zero mean value. The 2-D surface height spectrum is given by

$$W(K_x, K_y) = \frac{l_{cx} l_{cy} \sigma_z^2}{4\pi} \exp\left(-\frac{K_x^2 l_{cx}^2}{4} - \frac{K_y^2 l_{cy}^2}{4}\right) \quad (1)$$

where l_{cx} and l_{cy} are the correlation lengths in the $\hat{\mathbf{x}}$ and $\hat{\mathbf{y}}$ directions, respectively, K_x and K_y are the spatial frequencies in the $\hat{\mathbf{x}}$ and $\hat{\mathbf{y}}$ directions, respectively, and σ_z is the surface height standard deviation. The incident wave is tapered so that the illuminated rough surface can be confined to the surface area $L_x \times L_y$. The sources of the tapered incident wave are in the domain $\mathcal{D}_1(\epsilon_1, \mu_1)$, which is usually free space, with permittivity ϵ_1 and permeability μ_1. The PEC object occupies the domain $\mathcal{D}_3$ bounded by Γ_o. It is buried in the dielectric domain $\mathcal{D}_2(\epsilon_2, \mu_2)$, at a depth d, under the mean plane of the rough surface Γ_s. The outward unit normal vector to the surface Γ_s (pointing into the domain $\mathcal{D}_1$) is denoted $\hat{\mathbf{n}}_s$ while the outward unit normal vector to the surface Γ_o (pointing into the domain $\mathcal{D}_2$) is denoted $\hat{\mathbf{n}}_o$.

B. Rigorous PMCHW-EFIE Formulation

The analysis of EM scattering from a PEC object buried under a rough surface using the equivalence principle leads to a set of field integral equations whose unknowns are the current densities defined on the boundaries of the rough surface (Γ_s) and the buried object (Γ_o), as illustrated in Fig. 2. From these integral equations, numerous formulations are developed. Here, the PMCHW integral equations, which combines EFIE and MFIE on both sides of the rough surface, and the EFIE established on the boundary of the buried PEC object are selected

$$-\left[\overline{\mathbf{E}}_1^{inc}(\overline{\mathbf{r}})\right]_{\tan} = \left[(\eta_1 \mathcal{L}_1 + \eta_2 \mathcal{L}_2)(\overline{\mathbf{J}}_s)(\overline{\mathbf{r}}, \overline{\mathbf{r}}')\right]_{\tan}$$
$$-\left[(\mathcal{K}_1 + \mathcal{K}_2)(\overline{\mathbf{M}}_s)(\overline{\mathbf{r}}, \overline{\mathbf{r}}')\right]_{\tan}$$
$$-\left[\eta_2 \mathcal{L}_2(\overline{\mathbf{J}}_o)(\overline{\mathbf{r}}, \overline{\mathbf{r}}')\right]_{\tan} \quad (2a)$$

$$-\left[\overline{\mathbf{H}}_1^{inc}(\overline{\mathbf{r}})\right]_{\tan} = \left[(\mathcal{K}_1 + \mathcal{K}_2)(\overline{\mathbf{J}}_s)(\overline{\mathbf{r}}, \overline{\mathbf{r}}')\right]_{\tan}$$
$$+\left[\left(\frac{\mathcal{L}_1}{\eta_1} + \frac{\mathcal{L}_2}{\eta_2}\right)(\overline{\mathbf{M}}_s)(\overline{\mathbf{r}}, \overline{\mathbf{r}}')\right]_{\tan}$$
$$-\left[\mathcal{K}_2(\overline{\mathbf{J}}_o)(\overline{\mathbf{r}}, \overline{\mathbf{r}}')\right]_{\tan} \quad (2b)$$

$$\mathbf{0} = \left[-\eta_2 \mathcal{L}_2(\overline{\mathbf{J}}_s)(\overline{\mathbf{r}}, \overline{\mathbf{r}}')\right]_{\tan} + \left[\mathcal{K}_2(\overline{\mathbf{M}}_s)(\overline{\mathbf{r}}, \overline{\mathbf{r}}')\right]_{\tan}$$
$$+ \left[\eta_2 \mathcal{L}_2(\overline{\mathbf{J}}_o)(\overline{\mathbf{r}}, \overline{\mathbf{r}}')\right]_{\tan}. \quad (2c)$$

where $\overline{\mathbf{J}}_s$ and $\overline{\mathbf{M}}_s$ are the electric and magnetic current densities, respectively, on Γ_s, $\overline{\mathbf{J}}_o$ is the electric current density on Γ_o, and η_i is the complex impedance of the domain $\mathcal{D}_i$ defined as

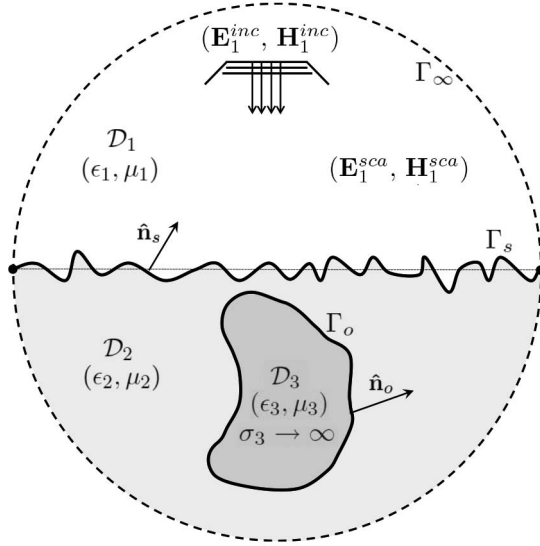$$\eta_i = \sqrt{\frac{\mu_i}{\epsilon_i}} \quad (3)$$

Fig. 1. Geometry of the scattering problem of a 3-D arbitrarily-shaped PEC object (bounded by Γ_o) buried under a 2-D random dielectric rough surface (with profile Γ_s).

Fig. 2. Equivalent scattering problem associated with the problem geometry of Fig. 1.

and

$$\epsilon_i = \epsilon_0 \epsilon_i^r = \epsilon_0 \left(\epsilon_i' - j \frac{\sigma_i}{\omega \epsilon_0} \right) \tag{4a}$$

$$\mu_i = \mu_0 \tag{4b}$$

where ϵ_i^r and σ_i are the relative permittivity and the conductivity of the domain $\mathcal{D}_i$, respectively, ϵ_0 and μ_0 are the vacuum permittivity and permeability, respectively, and ω is the angular frequency. The operators $\mathcal{L}_i$ and $\mathcal{K}_i$ are defined as

$$\mathcal{L}_i \left(\overline{\mathbf{X}} \right) \left(\overline{\mathbf{r}}, \overline{\mathbf{r}}' \right) = -jk_i \int_\Gamma \mathrm{G}_i \left(\overline{\mathbf{r}}, \overline{\mathbf{r}}' \right) \overline{\mathbf{X}} \left(\overline{\mathbf{r}}' \right) d\Gamma'$$
$$- \frac{j}{k_i} \nabla \int_\Gamma \mathrm{G}_i \left(\overline{\mathbf{r}}, \overline{\mathbf{r}}' \right) \nabla' \cdot \overline{\mathbf{X}} \left(\overline{\mathbf{r}}' \right) d\Gamma' \tag{5a}$$

$$\mathcal{K}_i \left(\overline{\mathbf{X}} \right) \left(\overline{\mathbf{r}}, \overline{\mathbf{r}}' \right) = \int_\Gamma \overline{\mathbf{X}} \left(\overline{\mathbf{r}}' \right) \times \nabla' \mathrm{G}_i \left(\overline{\mathbf{r}}, \overline{\mathbf{r}}' \right) d\Gamma' \tag{5b}$$

where k_i and $\mathrm{G}_i \left(\overline{\mathbf{r}}, \overline{\mathbf{r}}' \right)$ are the wavenumber and the scalar Green's function associated with the domain $\mathcal{D}_i$, respectively, Γ is the integration surface, and finally $\overline{\mathbf{X}}$ is the input variable of the operators representing surface current densities $\overline{\mathbf{J}}_s$, $\overline{\mathbf{J}}_o$, or $\overline{\mathbf{M}}_s$. The expression of the scalar Green's function in the domain $\mathcal{D}_i$ is given by

$$\mathrm{G}_i \left(\overline{\mathbf{r}}, \overline{\mathbf{r}}' \right) = \frac{e^{-jk_i R}}{4\pi R} \tag{6}$$

where $R = \sqrt{\left(x - x' \right)^2 + \left(y - y' \right)^2 + \left(z - z' \right)^2}$ is the distance between the observation $\overline{\mathbf{r}}$ and the source $\overline{\mathbf{r}}'$ locations.

C. Hybrid KA-EFIE Formulation

Since the field integral equations are linear, the superposition principle can reduce the solution of the original equivalent
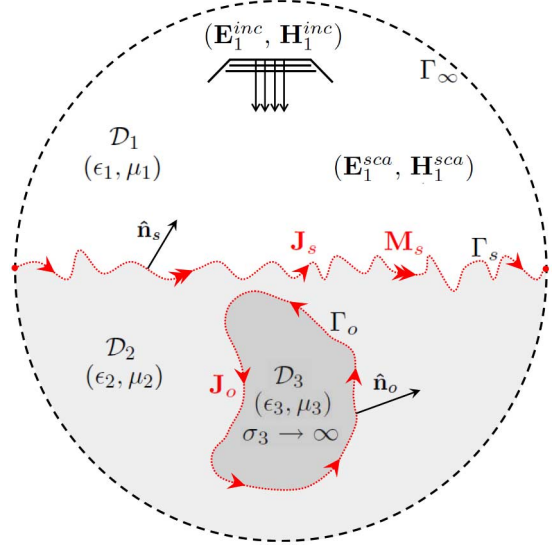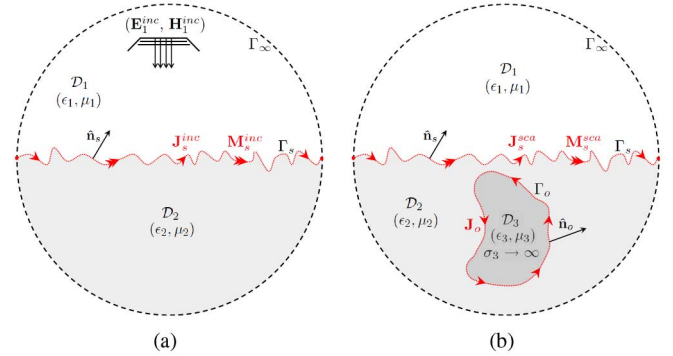

Fig. 3. Reduced equivalent scattering problems associated with the application of superposition principle to Fig. 2.

scattering problem (Fig. 2) to the sum of solutions of simpler equivalent scattering problems (Fig. 3). Thus, the electric and magnetic current densities ($\overline{\mathbf{J}}_s$ and $\overline{\mathbf{M}}_s$) on the rough surface, Γ_s, can be represented by a linear combination of two independent solutions as

$$\overline{\mathbf{J}}_s = \overline{\mathbf{J}}_s^{inc} + \overline{\mathbf{J}}_s^{sca} \tag{7a}$$

$$\overline{\mathbf{M}}_s = \overline{\mathbf{M}}_s^{inc} + \overline{\mathbf{M}}_s^{sca}. \tag{7b}$$

The electric and magnetic current densities ($\overline{\mathbf{J}}_s^{inc}, \overline{\mathbf{M}}_s^{inc}$) are generated by the incident-tapered wave in the absence of the buried object [Fig. 3(a)] and the electric and magnetic current densities ($\overline{\mathbf{J}}_s^{sca}, \overline{\mathbf{M}}_s^{sca}$) are due to the fields scattered by the buried object in the absence of the incident wave sources [Fig. 3(b)].

The first step is then to compute the electric $\overline{\mathbf{J}}_s^{inc}$ and magnetic $\overline{\mathbf{M}}_s^{inc}$ current densities. This can be rigorously achieved by solving the PMCHW integral equations associated with the reduced equivalent scattering problem [Fig. 3(a)] using an

MoM. These integral equations are obtained from (2a) and (2b) by neglecting the electric current density $\overline{\mathbf{J}}_o$ as

$$-\left[\overline{\mathbf{E}}_1^{inc}(\overline{\mathbf{r}})\right]_{\tan} = \left[(\eta_1\mathcal{L}_1+\eta_2\mathcal{L}_2)\left(\overline{\mathbf{J}}_s^{inc}\right)(\overline{\mathbf{r}},\overline{\mathbf{r}}')\right]_{\tan}$$
$$-\left[(\mathcal{K}_1+\mathcal{K}_2)\left(\overline{\mathbf{M}}_s^{inc}\right)(\overline{\mathbf{r}},\overline{\mathbf{r}}')\right]_{\tan} \quad (8a)$$

$$-\left[\overline{\mathbf{H}}_1^{inc}(\overline{\mathbf{r}})\right]_{\tan} = \left[(\mathcal{K}_1+\mathcal{K}_2)\left(\overline{\mathbf{J}}_s^{inc}\right)(\overline{\mathbf{r}},\overline{\mathbf{r}}')\right]_{\tan}$$
$$+\left[\left(\frac{\mathcal{L}_1}{\eta_1}+\frac{\mathcal{L}_2}{\eta_2}\right)\left(\overline{\mathbf{M}}_s^{inc}\right)(\overline{\mathbf{r}},\overline{\mathbf{r}}')\right]_{\tan}. \quad (8b)$$

Nevertheless, solving the matrix equation arising from an MoM discretization of (8) is prohibitive in terms of CPU time and storage requirements for electrically large rough surfaces. Therefore, the current-based KA that analytically gives the electric and magnetic current densities (without solving the MoM matrix equation) is used to reduce the computational cost.

In this context, the incident fields are locally decomposed into their transverse electric (TE) and transverse magnetic (TM) components using the tangent plane as the interface in order to independently insert the Fresnel coefficients in the evaluation of the surface current densities. This is achieved according to an orthonormal basis $(\hat{\mathbf{p}}_i, \hat{\mathbf{q}}_i, \hat{\mathbf{k}}_i)$ defined at any point $\overline{\mathbf{r}}$ on the rough surface with

$$\hat{\mathbf{q}}_i(\overline{\mathbf{r}}) = \frac{\hat{\mathbf{n}}_s(\overline{\mathbf{r}})\times\hat{\mathbf{k}}_i}{\|\hat{\mathbf{n}}_s(\overline{\mathbf{r}})\times\hat{\mathbf{k}}_i\|}; \quad \hat{\mathbf{p}}_i(\overline{\mathbf{r}}) = \hat{\mathbf{q}}_i(\overline{\mathbf{r}})\times\hat{\mathbf{k}}_i \quad (9)$$

where the unit vectors $\hat{\mathbf{q}}_i$ and $\hat{\mathbf{p}}_i$ are the local perpendicular and parallel polarization vectors, respectively, and $\hat{\mathbf{k}}_i = \frac{\overline{\mathbf{k}}_i}{k_1}$ is the unit incident wave vector.

Thereby, the KA-based current densities at any point $\overline{\mathbf{r}}$ on the rough surface can be expressed by the following equations:

$$\overline{\mathbf{J}}_s^{inc}(\overline{\mathbf{r}}) = \xi^{\mathcal{D}_1}(\overline{\mathbf{r}})$$
$$\left\{\left(\overline{\mathbf{H}}_1^{inc}(\overline{\mathbf{r}})\cdot\hat{\mathbf{q}}_i(\overline{\mathbf{r}})\right)\left(1+R_{TM}^{\mathcal{D}_1}\right)[\hat{\mathbf{n}}_s(\overline{\mathbf{r}})\times\hat{\mathbf{q}}_i(\overline{\mathbf{r}})]\right.$$
$$\left. -\left(\overline{\mathbf{H}}_1^{inc}(\overline{\mathbf{r}})\cdot\hat{\mathbf{p}}_i(\overline{\mathbf{r}})\right)\cos\theta_{li}\left(1-R_{TE}^{\mathcal{D}_1}\right)\hat{\mathbf{q}}_i(\overline{\mathbf{r}})\right\} \quad (10a)$$

$$\overline{\mathbf{M}}_s^{inc}(\overline{\mathbf{r}}) = \xi^{\mathcal{D}_1}(\overline{\mathbf{r}})$$
$$\left\{\left(\overline{\mathbf{E}}_1^{inc}(\overline{\mathbf{r}})\cdot\hat{\mathbf{p}}_i(\overline{\mathbf{r}})\right)\cos\theta_{li}\left(1-R_{TM}^{\mathcal{D}_1}\right)\hat{\mathbf{q}}_i(\overline{\mathbf{r}})\right.$$
$$\left. -\left(\overline{\mathbf{E}}_1^{inc}(\overline{\mathbf{r}})\cdot\hat{\mathbf{q}}_i(\overline{\mathbf{r}})\right)\left(1+R_{TE}^{\mathcal{D}_1}\right)[\hat{\mathbf{n}}_s(\overline{\mathbf{r}})\times\hat{\mathbf{q}}_i(\overline{\mathbf{r}})]\right\} \quad (10b)$$

where the local incident angle on the rough surface θ_{li} satisfies $\cos\theta_{li} = -\hat{\mathbf{n}}_s(\overline{\mathbf{r}})\cdot\hat{\mathbf{k}}_i$ and the geometrical optics (GO) shadowing function $\xi^{\mathcal{D}_1}(\overline{\mathbf{r}})$ satisfies

$$\xi^{\mathcal{D}_1}(\overline{\mathbf{r}}) = \begin{cases} 1, & \text{if } \hat{\mathbf{n}}_s(\overline{\mathbf{r}})\cdot\hat{\mathbf{k}}_i < 0; \\ 0, & \text{if } \hat{\mathbf{n}}_s(\overline{\mathbf{r}})\cdot\hat{\mathbf{k}}_i \geq 0. \end{cases} \quad (11)$$

The local Fresnel reflection coefficients of TE polarization $R_{TE}^{\mathcal{D}_1}$ and TM polarization $R_{TM}^{\mathcal{D}_1}$ are given by

$$R_{TE}^{\mathcal{D}_1} = \frac{\cos\theta_{li}-\sqrt{\epsilon_2^r-\sin^2\theta_{li}}}{\cos\theta_{li}+\sqrt{\epsilon_2^r-\sin^2\theta_{li}}} \quad (12a)$$

$$R_{TM}^{\mathcal{D}_1} = \frac{\epsilon_2^r\cos\theta_{li}-\sqrt{\epsilon_2^r-\sin^2\theta_{li}}}{\epsilon_2^r\cos\theta_{li}+\sqrt{\epsilon_2^r-\sin^2\theta_{li}}}. \quad (12b)$$

In order to reconstruct the final solution, the second step deals with the computation of the electric and magnetic current densities $(\overline{\mathbf{J}}_s^{sca}, \overline{\mathbf{M}}_s^{sca})$ induced by the electric and magnetic fields $(\eta_2\mathcal{L}_2(\overline{\mathbf{J}}_o)(\overline{\mathbf{r}},\overline{\mathbf{r}}'), \mathcal{K}_2(\overline{\mathbf{J}}_o)(\overline{\mathbf{r}},\overline{\mathbf{r}}'))$ scattered by the buried object. These current densities can be rigorously determined by solving the PMCHW integral equations associated with the reduced equivalent scattering problem [Fig. 3(b)]. These PMCHW integral equations are obtained from (2a) and (2b) by neglecting the electric and magnetic incident fields and only leaving the excitation due to the fields scattered by the buried object as

$$\left[\eta_2\mathcal{L}_2(\overline{\mathbf{J}}_o)(\overline{\mathbf{r}},\overline{\mathbf{r}}')\right]_{\tan} = \left[(\eta_1\mathcal{L}_1+\eta_2\mathcal{L}_2)\left(\overline{\mathbf{J}}_s^{sca}\right)(\overline{\mathbf{r}},\overline{\mathbf{r}}')\right]_{\tan}$$
$$-\left[(\mathcal{K}_1+\mathcal{K}_2)\left(\overline{\mathbf{M}}_s^{sca}\right)(\overline{\mathbf{r}},\overline{\mathbf{r}}')\right]_{\tan} \quad (13a)$$

$$\left[\mathcal{K}_2(\overline{\mathbf{J}}_o)(\overline{\mathbf{r}},\overline{\mathbf{r}}')\right]_{\tan} = \left[(\mathcal{K}_1+\mathcal{K}_2)\left(\overline{\mathbf{J}}_s^{sca}\right)(\overline{\mathbf{r}},\overline{\mathbf{r}}')\right]_{\tan}$$
$$+\left[\left(\frac{\mathcal{L}_1}{\eta_1}+\frac{\mathcal{L}_2}{\eta_2}\right)\left(\overline{\mathbf{M}}_s^{sca}\right)(\overline{\mathbf{r}},\overline{\mathbf{r}}')\right]_{\tan}. \quad (13b)$$

However, in order to avoid solving the resulting MoM matrix equation and further reduce the computational cost, we again use the KA to obtain the analytic expressions of electric and magnetic current densities $(\overline{\mathbf{J}}_s^{sca}, \overline{\mathbf{M}}_s^{sca})$ as

$$\overline{\mathbf{J}}_s^{sca}(\overline{\mathbf{r}}) = \xi^{\mathcal{D}_2}(\overline{\mathbf{r}})$$
$$\left\{\left(\mathcal{K}_2(\overline{\mathbf{J}}_o)(\overline{\mathbf{r}},\overline{\mathbf{r}}')\cdot\hat{\mathbf{p}}_s(\overline{\mathbf{r}})\right)\cos\theta_{ls}\left(1-R_{TE}^{\mathcal{D}_2}\right)\hat{\mathbf{q}}_s(\overline{\mathbf{r}})\right.$$
$$\left. +\left(\mathcal{K}_2(\overline{\mathbf{J}}_o)(\overline{\mathbf{r}},\overline{\mathbf{r}}')\cdot\hat{\mathbf{q}}_s(\overline{\mathbf{r}})\right)\left(1+R_{TM}^{\mathcal{D}_2}\right)[\hat{\mathbf{n}}_s(\overline{\mathbf{r}})\times\hat{\mathbf{q}}_s(\overline{\mathbf{r}})]\right\} \quad (14a)$$

$$\overline{\mathbf{M}}_s^{sca}(\overline{\mathbf{r}}) = -\xi^{\mathcal{D}_2}(\overline{\mathbf{r}})$$
$$\left\{\left(\eta_2\mathcal{L}_2(\overline{\mathbf{J}}_o)(\overline{\mathbf{r}},\overline{\mathbf{r}}')\cdot\hat{\mathbf{p}}_s(\overline{\mathbf{r}})\right)\cos\theta_{ls}\left(1-R_{TM}^{\mathcal{D}_2}\right)\hat{\mathbf{q}}_s(\overline{\mathbf{r}})\right.$$
$$\left. +\left(\eta_2\mathcal{L}_2(\overline{\mathbf{J}}_o)(\overline{\mathbf{r}},\overline{\mathbf{r}}')\cdot\hat{\mathbf{q}}_s(\overline{\mathbf{r}})\right)\left(1+R_{TE}^{\mathcal{D}_2}\right)[\hat{\mathbf{n}}_s(\overline{\mathbf{r}})\times\hat{\mathbf{q}}_s(\overline{\mathbf{r}})]\right\} \quad (14b)$$

where the local incident angle on the rough surface (from the bottom) θ_{ls} satisfies $\cos\theta_{ls} = \hat{\mathbf{n}}_s(\overline{\mathbf{r}})\cdot\hat{\mathbf{r}}_s$ (with $\hat{\mathbf{r}}_s = \frac{\overline{\mathbf{r}}-\overline{\mathbf{r}}'}{\|\overline{\mathbf{r}}-\overline{\mathbf{r}}'\|}$), the unit vectors $\hat{\mathbf{q}}_s$ and $\hat{\mathbf{p}}_s$ are the local perpendicular and parallel polarization vectors given by

$$\hat{\mathbf{q}}_s(\overline{\mathbf{r}}) = \frac{\hat{\mathbf{n}}_s(\overline{\mathbf{r}})\times\hat{\mathbf{r}}_s}{\|\hat{\mathbf{n}}_s(\overline{\mathbf{r}})\times\hat{\mathbf{r}}_s\|}; \quad \hat{\mathbf{p}}_s(\overline{\mathbf{r}}) = \hat{\mathbf{q}}_s(\overline{\mathbf{r}})\times\hat{\mathbf{r}}_s \quad (15)$$

the GO shadowing function, $\xi^{\mathcal{D}_2}(\overline{\mathbf{r}})$, satisfies

$$\xi^{\mathcal{D}_2}(\overline{\mathbf{r}}) = \begin{cases} 1, & \text{if } \hat{\mathbf{n}}_s(\overline{\mathbf{r}})\cdot\hat{\mathbf{r}}_s > 0; \\ 0, & \text{if } \hat{\mathbf{n}}_s(\overline{\mathbf{r}})\cdot\hat{\mathbf{r}}_s \leq 0 \end{cases} \quad (16)$$

and the local Fresnel reflection coefficients of TE polarization $R_{\text{TE}}^{\mathcal{D}_2}$ and TM polarization $R_{\text{TM}}^{\mathcal{D}_2}$ are given by

$$R_{\text{TE}}^{\mathcal{D}_2} = \frac{\sqrt{\epsilon_2^r}\cos\theta_{ls} - \sqrt{1 - \epsilon_2^r\sin^2\theta_{ls}}}{\sqrt{\epsilon_2^r}\cos\theta_{ls} + \sqrt{1 - \epsilon_2^r\sin^2\theta_{ls}}} \tag{17a}$$

$$R_{\text{TM}}^{\mathcal{D}_2} = \frac{\cos\theta_{ls} - \sqrt{\epsilon_2^r}\sqrt{1 - \epsilon_2^r\sin^2\theta_{ls}}}{\cos\theta_{ls} + \sqrt{\epsilon_2^r}\sqrt{1 - \epsilon_2^r\sin^2\theta_{ls}}}. \tag{17b}$$

Finally, by adding (10) and (14) and using the EFIE in (2c), the KA-EFIE formulation (three equations) for a PEC object buried beneath a dielectric rough surface is obtained. It is also worthwhile to point out that the rigorous computation of the incident current densities ($\overline{\mathbf{J}}_s^{inc}$, $\overline{\mathbf{M}}_s^{inc}$) and the scattered current densities ($\overline{\mathbf{J}}_s^{sca}$, $\overline{\mathbf{M}}_s^{sca}$) by solving the integral equations (8), (13), and (2c) using an MoM leads to the same result as that of the original PMCHW-EFIE formulation given by (2). In fact, summing up (8) and (13) leads to (2a) and (2b).

On the other hand, two other formulations can be derived. The first one is the PMCHW-KA-EFIE formulation in which the PMCHW integral equations (8) are used to compute the incident current densities ($\overline{\mathbf{J}}_s^{inc}$, $\overline{\mathbf{M}}_s^{inc}$), the current-based KA (14) is used to compute the scattered current densities ($\overline{\mathbf{J}}_s^{sca}$, $\overline{\mathbf{M}}_s^{sca}$), and the EFIE (2c) is applied to compute the electric current density ($\overline{\mathbf{J}}_o$) on the buried object. The second one is the KA-PMCHW-EFIE formulation in which the current-based KA (10) is used to compute the incident current densities ($\overline{\mathbf{J}}_s^{inc}$, $\overline{\mathbf{M}}_s^{inc}$), the PMCHW integral equations (13) are used to compute the scattered current densities ($\overline{\mathbf{J}}_s^{sca}$, $\overline{\mathbf{M}}_s^{sca}$), and the EFIE (2c) is applied to compute the electric current density ($\overline{\mathbf{J}}_o$) on the buried object. These formulations which involve a tradeoff between the computational cost and the accuracy of the solution can also be used.

Once the electric and magnetic current densities ($\overline{\mathbf{J}}_s$, $\overline{\mathbf{M}}_s$) are determined through the PMCHW-EFIE formulation (2) or the KA-EFIE formulation, the EM scattered field at any point $\overline{\mathbf{r}} \in \mathcal{D}_1$ can be evaluated using the following expressions:

$$\overline{\mathbf{E}}_1^{sca}(\overline{\mathbf{r}}) = \eta_1\mathcal{L}_1\left(\overline{\mathbf{J}}_s\right)(\overline{\mathbf{r}},\overline{\mathbf{r}}') - \mathcal{K}_1\left(\overline{\mathbf{M}}_s\right)(\overline{\mathbf{r}},\overline{\mathbf{r}}') \tag{18a}$$

$$\overline{\mathbf{H}}_1^{sca}(\overline{\mathbf{r}}) = \frac{\mathcal{L}_1}{\eta_1}\left(\overline{\mathbf{M}}_s\right)(\overline{\mathbf{r}},\overline{\mathbf{r}}') + \mathcal{K}_1\left(\overline{\mathbf{J}}_s\right)(\overline{\mathbf{r}},\overline{\mathbf{r}}'). \tag{18b}$$

In the far-field zone, the integral operators $\mathcal{L}_1$ and $\mathcal{K}_1$ can be simplified to $\mathcal{L}_1^{\text{FF}}$ and $\mathcal{K}_1^{\text{FF}}$ as

$$\mathcal{L}_1^{\text{FF}}(\overline{\mathbf{X}}) = \frac{jk_1 e^{-jk_1 r}}{4\pi r}\hat{\mathbf{k}}^s \times \hat{\mathbf{k}}^s \times \int_{\Gamma_s}\overline{\mathbf{X}}(\overline{\mathbf{r}}')e^{jk_1\overline{\mathbf{r}}'\cdot\hat{\mathbf{k}}^s}d\Gamma_s' \tag{19a}$$

$$\mathcal{K}_1^{\text{FF}}(\overline{\mathbf{X}}) = -\frac{jk_1 e^{-jk_1 r}}{4\pi r}\hat{\mathbf{k}}^s \times \int_{\Gamma_s}\overline{\mathbf{X}}(\overline{\mathbf{r}}')e^{jk_1\overline{\mathbf{r}}'\cdot\hat{\mathbf{k}}^s}d\Gamma_s' \tag{19b}$$

where $\hat{\mathbf{k}}^s$ is the scattering direction and r is the distance from the origin to the receiver position.

The scattered field is afterward needed for the computation of the normalized radar cross-section (NRCS; bistatic scattering coefficient) which is defined as

$$\text{NRCS}_{pq}(\hat{\mathbf{k}}_i,\hat{\mathbf{k}}_s) = \lim_{r\to\infty} r^2\frac{\left|\overline{\mathbf{E}}_1^{sca}(\overline{\mathbf{r}})\cdot\hat{\mathbf{p}}^s\right|^2}{2\eta_1 P_q^{inc}} \tag{20}$$

where q and p indicate the polarization of the incident and scattered fields, respectively, $\hat{\mathbf{p}}^s$ is the scattering polarization unit vector and P_q^{inc} is the the incident beam power which its analytical expression is given by

$$P_q^{inc} = \frac{\cos\theta_i}{2\eta_1}\frac{\pi}{2}g^2\left[1 - \frac{1 + \cos^2\theta_i + 2\tan^2\theta_i}{2k_1^2 g^2\cos^2\theta_i}\right] \tag{21}$$

with g the tapering parameter of the incident wave and θ_i its incidence angle.

III. DISCRETIZATION OF THE KA-EFIE FORMULATION

The hybrid KA-EFIE formulation for the scattering from a PEC object buried beneath a dielectric rough surface can be implemented numerically by converting the continuous equations to a matrix equation with the most versatile numerical technique referred to as the MoM. The electric and magnetic currents on the surface Γ_s are expanded in terms of a known set of N_s basis functions $\overline{\mathbf{f}}_s(\overline{\mathbf{r}})$ and the electric current on the surface Γ_o of the buried object is expanded in terms of a known set of N_o basis functions $\overline{\mathbf{f}}_o(\overline{\mathbf{r}})$ as

$$\overline{\mathbf{J}}_s(\overline{\mathbf{r}}) \approx \sum_{j=1}^{N_s} J_s^j\overline{\mathbf{f}}_j^s(\overline{\mathbf{r}}) \quad \forall\overline{\mathbf{r}}\in\Gamma_s \tag{22a}$$

$$\overline{\mathbf{M}}_s(\overline{\mathbf{r}}) \approx \sum_{j=1}^{N_s} M_s^j\overline{\mathbf{f}}_j^s(\overline{\mathbf{r}}) \quad \forall\overline{\mathbf{r}}\in\Gamma_s \tag{22b}$$

$$\overline{\mathbf{J}}_o(\overline{\mathbf{r}}) \approx \sum_{n=1}^{N_o} J_o^n\overline{\mathbf{f}}_n^o(\overline{\mathbf{r}}) \quad \forall\overline{\mathbf{r}}\in\Gamma_o \tag{22c}$$

where J_s^j and M_s^j are the unknown weights of the expansions for the electric $\overline{\mathbf{J}}_s(\overline{\mathbf{r}})$ and magnetic $\overline{\mathbf{M}}_s(\overline{\mathbf{r}})$ current densities, respectively, and J_o^n is the unknown weight of the expansion for the electric current density $\overline{\mathbf{J}}_o(\overline{\mathbf{r}})$. Next, for the testing procedure, the conventional Galerkin's method is applied on the surface Γ_o: the test functions are then chosen equal to the basis functions. However, on the surface Γ_s, a point matching method [26] is applied: the test function is defined as $\overline{\mathbf{t}}_s^j = \delta(\overline{\mathbf{r}} - \overline{\mathbf{r}}^j)\hat{\tau}_s^j$, where δ is the 3-D Dirac delta function, $\overline{\mathbf{r}}^j$ is the midpoint of edge j and $\hat{\tau}_s^j$ is a unit vector perpendicular to the edge and parallel to the triangular facet. The MoM discretization of KA-EFIE formulation yields to a system of $N = 2N_s + N_o$ linear equations that are cast into a matrix equation as follows:

$$\begin{bmatrix} \mathbf{R}_s & \mathbf{R}_{so} \\ \mathbf{Z}_{os} & \mathbf{Z}_o \end{bmatrix}\begin{bmatrix} \mathbf{I}_s \\ \mathbf{I}_o \end{bmatrix} = \begin{bmatrix} \mathbf{I}_s^i \\ \mathbf{0} \end{bmatrix} \tag{23}$$

where

$$\mathbf{R}_s = \begin{bmatrix} \mathbf{I} & \mathbf{0} \\ \mathbf{0} & \mathbf{I} \end{bmatrix}$$ is a self-reaction matrix of size $[2N_s \times 2N_s]$ and $\mathbf{I}$ is an identity matrix.

$\mathbf{R}_{so} = \begin{bmatrix} \mathbf{R}_{so}^{ee} \\ \mathbf{R}_{so}^{me} \end{bmatrix}$ is a mutual-reaction matrix of size $[2N_s \times N_o]$ which relates the electric and magnetic current densities on the rough surface to the electric current density on the buried object

$$\mathbf{R}_{so}^{ee}(m,n) =$$
$$-\xi^{\mathcal{D}_2} \left\{ \left(\hat{\mathbf{q}}_s \cdot \mathcal{K}_2 \left(\overline{\mathbf{f}}_o^n \right) \right) \left(1 + R_{\mathrm{TM}}^{\mathcal{D}_2} \right) \left(\hat{\boldsymbol{\tau}}_s^m \cdot [\hat{\mathbf{n}}_s \times \hat{\mathbf{q}}_s] \right) \right.$$
$$\left. + \left(\hat{\mathbf{p}}_s \cdot \mathcal{K}_2 \left(\overline{\mathbf{f}}_o^n \right) \right) \cos\theta_{ls} \left(1 - R_{\mathrm{TE}}^{\mathcal{D}_2} \right) \left(\hat{\boldsymbol{\tau}}_s^m \cdot \hat{\mathbf{q}}_s \right) \right\}$$
$$(24a)$$

$$\mathbf{R}_{so}^{me}(m,n) =$$
$$+\xi^{\mathcal{D}_2} \left\{ \eta_2 \left(\hat{\mathbf{p}}_s \cdot \mathcal{L}_2 \left(\overline{\mathbf{f}}_o^n \right) \right) \cos\theta_{ls} \left(1 - R_{\mathrm{TM}}^{\mathcal{D}_2} \right) \left(\hat{\boldsymbol{\tau}}_s^m \cdot \hat{\mathbf{q}}_s \right) \right.$$
$$\left. + \eta_2 \left(\hat{\mathbf{q}}_s \cdot \mathcal{L}_2 \left(\overline{\mathbf{f}}_o^n \right) \right) \left(1 + R_{\mathrm{TE}}^{\mathcal{D}_2} \right) \left(\hat{\boldsymbol{\tau}}_s^m \cdot [\hat{\mathbf{n}}_s \times \hat{\mathbf{q}}_s] \right) \right\}.$$
$$(24b)$$

$\mathbf{Z}_{os} = \begin{bmatrix} \mathbf{Z}_{os}^{ee} & \mathbf{Z}_{os}^{em} \end{bmatrix}$ is a mutual-impedance matrix of size $[N_o \times 2N_s]$ which characterizes the scattering from the rough surface to the buried object

$$\mathbf{Z}_{os}^{ee} = -\eta_2 \int_{\Gamma_o} \overline{\mathbf{f}}_o \cdot \mathcal{L}_2 \left(\overline{\mathbf{f}}_s \right) d\Gamma_o \qquad (25a)$$

$$\mathbf{Z}_{os}^{em} = \int_{\Gamma_o} \overline{\mathbf{f}}_o \cdot \mathcal{K}_2 \left(\overline{\mathbf{f}}_s \right) d\Gamma_o. \qquad (25b)$$

$\mathbf{Z}_o = \mathbf{Z}_o^{ee}$ is a self-impedance matrix of size $[N_o \times N_o]$ characterizing the local interactions on the buried object

$$\mathbf{Z}_o^{ee} = \eta_2 \int_{\Gamma_o} \overline{\mathbf{f}}_o \cdot \mathcal{L}_2 \left(\overline{\mathbf{f}}_o \right) d\Gamma_o. \qquad (26)$$

$\mathbf{I}_s^i = \begin{bmatrix} \mathbf{J}_s^i \\ \mathbf{M}_s^i \end{bmatrix}$ is a vector of size $[2N_s \times 1]$ which represents the initial current densities due to the incident tapered wave

$$\mathbf{J}_s^i(m) = \xi^{\mathcal{D}_1} \left\{ \left(\hat{\mathbf{q}}_i \cdot \overline{\mathbf{H}}_1^{inc} \right) \left(1 + R_{\mathrm{TM}}^{\mathcal{D}_1} \right) \left(\hat{\boldsymbol{\tau}}_s^m \cdot [\hat{\mathbf{n}}_s \times \hat{\mathbf{q}}_i] \right) \right.$$
$$\left. - \left(\hat{\mathbf{p}}_i \cdot \overline{\mathbf{H}}_1^{inc} \right) \cos\theta_{li} \left(1 - R_{\mathrm{TE}}^{\mathcal{D}_1} \right) \left(\hat{\boldsymbol{\tau}}_s^m \cdot \hat{\mathbf{q}}_i \right) \right\} \quad (27a)$$

$$\mathbf{M}_s^i(m) = \xi^{\mathcal{D}_1} \left\{ \left(\hat{\mathbf{p}}_i \cdot \overline{\mathbf{E}}_1^{inc} \right) \cos\theta_{li} \left(1 - R_{\mathrm{TM}}^{\mathcal{D}_1} \right) \left(\hat{\boldsymbol{\tau}}_s^m \cdot \hat{\mathbf{q}}_i \right) \right.$$
$$\left. - \left(\hat{\mathbf{q}}_i \cdot \overline{\mathbf{E}}_1^{inc} \right) \left(1 + R_{\mathrm{TE}}^{\mathcal{D}_1} \right) \left(\hat{\boldsymbol{\tau}}_s^m \cdot [\hat{\mathbf{n}}_s \times \hat{\mathbf{q}}_i] \right) \right\}. \quad (27b)$$

Because of the computation of the scattered fields only requires the explicit knowledge of the current densities on the surface Γ_s, the matrix equation can be rearranged as

$$\mathbf{I}_s = \left(\mathbf{I} - \mathbf{R}_s^{-1} \mathbf{R}_{so} \mathbf{Z}_o^{-1} \mathbf{Z}_{os} \right)^{-1} \mathbf{R}_s^{-1} \mathbf{I}_s^i. \qquad (28)$$

Given that the matrix $\mathbf{R}_s$ is an identity matrix the above equation can be simplified as

$$\mathbf{I}_s = \left(\mathbf{I} - \mathbf{R}_{so} \mathbf{Z}_o^{-1} \mathbf{Z}_{os} \right)^{-1} \mathbf{I}_s^i. \qquad (29)$$

This equation can be solved by means of the iterative PILE method as follows:

$$\mathbf{I}_s^{(P_{\mathrm{PILE}})} = \sum_{p=0}^{p=P_{\mathrm{PILE}}} \left(\mathbf{R}_{so} \mathbf{Z}_o^{-1} \mathbf{Z}_{os} \right)^p \mathbf{I}_s^i. \qquad (30)$$

It should be noted that (30) is only valid when the spectral radius (modulus of its highest eigenvalue) of the matrix in the bracket is strictly smaller than one. The order $p = P_{\mathrm{PILE}}$ is obtained according to the following convergence criterion:

$$\frac{\| \mathbf{I}_s^{(p)} - \mathbf{I}_s^{(p-1)} \|_2}{\| \mathbf{I}_s^{(p)} \|_2} < 1\%. \qquad (31)$$

The PILE-based algorithm for solving KA-EFIE matrix equation is as follows.

- Initialization step
  - Compute and store upper $\mathbf{L}_o^{ee}$ and lower $\mathbf{U}_o^{ee}$ triangular matrices of the self-impedance matrix, $\mathbf{Z}_o^{ee}$, of the buried object.
  - Compute the incident electric $\mathbf{J}_s^i$ and magnetic $\mathbf{M}_s^i$ current densities on the dielectric rough surface due to the incident wave illumination

$$\mathbf{J}_s^{(0)} = \mathbf{J}_s^i \qquad (32a)$$
$$\mathbf{M}_s^{(0)} = \mathbf{M}_s^i. \qquad (32b)$$

- Repeated ($n = P_{\mathrm{PILE}}$ times) steps until the convergence is reached
  1) Compute the electric field scattered $\mathbf{W}_o^e$ from the rough surface to the buried object

$$\mathbf{W}_o^e = \mathbf{Z}_{os}^{ee} \mathbf{J}_s^{(n)} + \mathbf{Z}_{os}^{em} \mathbf{M}_s^{(n)}. \qquad (33)$$

  2) Compute the electric current density on the buried object

$$\mathbf{I}_o^e = (\mathbf{U}_o^{ee})^{-1} \left((\mathbf{L}_o^{ee})^{-1} \mathbf{W}_o^e \right). \qquad (34)$$

  3) Compute the high-order electric and magnetic current densities on the dielectric rough surface due to the coupling interaction between the scatterers

$$\mathbf{J}_s^{(n+1)} = \mathbf{R}_{so}^{ee} \mathbf{I}_o^e + \mathbf{J}_s^{(n)} \qquad (35a)$$
$$\mathbf{M}_s^{(n+1)} = \mathbf{R}_{so}^{me} \mathbf{I}_o^e + \mathbf{M}_s^{(n)}. \qquad (35b)$$

  4) Check convergence criterion given by (31)
     - If satisfied: $P_{\mathrm{PILE}} = n + 1$ and the algorithm is stopped
     - Else increment n and go to step 1.

The complexities associated with the above PILE-based algorithm are $\mathcal{O}\left(N_o^3 + 2N_s + P_{\mathrm{PILE}}\left(N_o^2 + 4N_s N_o\right)\right)$ for operations and $\mathcal{O}\left(4N_s N_o + N_o^2\right)$ for memory storage. It is important to note that the complexities of the PILE-based algorithm solving the PMCHW-EFIE matrix equation are $\mathcal{O}(8N_s^3 + N_o^3 + 4N_s^2 + P_{\mathrm{PILE}}(4N_s^2 + N_o^2 + 4N_s N_o))$ for operations and $\mathcal{O}\left(4N_s^2\right)$ for memory storage. It is clear that solving the hybrid KA-EFIE using the PILE-based algorithm significantly reduces the computational cost.

Since the rough surface is often much larger than the buried object ($N_s \gg N_o$), the most time-consuming task is related to the matrix–vector products associated with the matrices $\mathbf{Z}_{os}^{ee}$, $\mathbf{Z}_{os}^{em}$, $\mathbf{R}_{so}^{ee}$, and $\mathbf{R}_{so}^{me}$ (steps 1 and 3). Therefore, the algebraic ACA is suitable to compress these matrices because their ranks

are often much less than their dimensions due to the smoothness of their elements (far-field interactions). The ACA can express a rectangular matrix $\mathbf{Z}$ of size $[M \times N]$ as a matrix–matrix product ($\mathbf{Z}_{M \times N} = \mathbf{U}_{M \times \kappa} \mathbf{V}_{\kappa \times N}$) where κ is the effective rank of $\mathbf{Z}$. The ACA algorithm converges after κ iterations for a given tolerance (typically an ACA threshold of 10^{-3} is often used) and requires the storage of only $\kappa (M + N)$ matrix elements. Its computational cost is $\mathcal{O}\left(\kappa^2 (M + N)\right)$ [27]. We define the matrix compression ratio as

$$\tau(\%) = \left(1 - \frac{\kappa (M + N)}{MN} \right) \times 100. \qquad (36)$$

The compression is efficient when $\kappa \ll \min(M, N)$ involving a compression ratio τ close to 100%. That way, the ACA improves the computational cost related to filling the matrix and calculating the matrix–vector product. Indeed, the matrix–vector product complexity is $\mathcal{O}\left(\kappa(M + N)\right)$ instead of the conventional $\mathcal{O}(MN)$.

The PILE-ACA-based algorithm for solving KA-EFIE matrix equation is obtained by modifying the equations in the steps 1 and 3 in the PILE-based algorithm as follows.

1) Compute the electric field scattered from the rough surface to the buried object

$$\mathbf{W}_o^e = \mathbf{U}_{os}^{ee} \left(\mathbf{V}_{os}^{ee} \mathbf{J}_s^{(n)} \right) + \mathbf{U}_{os}^{em} \left(\mathbf{V}_{os}^{em} \mathbf{M}_s^{(n)} \right). \quad (37)$$

2) Compute the high-order electric and magnetic current densities on the dielectric rough surface due to the coupling interaction between the scatterers

$$\mathbf{J}_s^{(n+1)} = \mathbf{U}_{so}^{ee} \left(\mathbf{V}_{so}^{ee} \mathbf{I}_o^e \right) + \mathbf{J}_s^{(n)} \qquad (38a)$$

$$\mathbf{M}_s^{(n+1)} = \mathbf{U}_{so}^{me} \left(\mathbf{V}_{so}^{me} \mathbf{I}_o^e \right) + \mathbf{M}_s^{(n)}. \qquad (38b)$$

The computational complexity of the above PILE-ACA-based algorithm is $\mathcal{O}\left(N_o^3 + 2N_s + P_{\text{PILE}}\left(N_o^2 + 4\kappa\left(N_s + N_o\right)\right)\right)$ with $\kappa = \frac{\kappa_{so}^{ee} + \kappa_{so}^{me} + \kappa_{os}^{ee} + \kappa_{os}^{em}}{4}$, the mean effective rank of the matrices $\mathbf{Z}_{os}^{ee}$, $\mathbf{Z}_{os}^{em}$, $\mathbf{R}_{so}^{ee}$, and $\mathbf{R}_{so}^{me}$. For memory storage, the complexity is reduced to $\mathcal{O}\left(4\kappa(N_s + N_o) + N_o^2\right)$.

IV. SIMULATION RESULTS

Several numerical simulations are considered to demonstrate the accuracy and effectiveness of KA-EFIE formulation when solved by PILE-based and PILE-ACA-based solvers. In our simulations, the length of the truncated rough surfaces is chosen to be $L = L_x = L_y = 10.60\lambda_1$, where λ_1 is the wavelength of the tapered incident wave with tapering parameter $g = L/4$, frequency $f = 300$ MHz ($\lambda_1 = 1$ m). It is important to underline that the Braunisch approximate 3-D vector-tapered wave assumes that $k_1 g(1 - \sin \theta_i) \gg 1$ and $g \gg |z|_{\max}$ [25], and it is, therefore, not valid for grazing incidence angles. The rough surface encloses a lossy medium with relative permittivity $\epsilon_2^r = 2 - j0.4$. As a PEC object, a horizontally PEC $0.2L \times 0.2L$ plate and then a PEC sphere of radius $0.4\lambda_1$ are buried at a depth d from the mean plane of rough surface ($z = 0$). The rough surface and the PEC plate are, respectively, discretized into 29 282 and 1250 triangular patches, which results in 45 506 (43 681 + 1825) edges and 89 187 (87 362 + 1825) unknowns.

The ACA threshold is set to 10^{-3}. The copolarized scattered field is evaluated in the far-field zone for the scattering direction $\hat{\mathbf{k}}_s(\theta_s, \phi_s)$ defined by θ_s varying from $-90°$ to $90°$ with an angular step of $1°$ and $\phi_s = \phi_i$.

In the legends, the results of the rigorous PMCHW-EFIE formulation are refereed to as "PILE" (taken as reference) and "PILE-ACA" when using the PILE-based and the PILE-ACA-based solvers, respectively. Similarly, the results of the hybrid KA-EFIE formulation are referred to as "KA-PILE" and "KA-PILE-ACA" when using the PILE-based and the PILE-ACA-based solvers, respectively. Within the brackets, the first number indicate the convergence order of the solver and the second term represents the relative error on current densities of the dielectric surface as defined by (31).

### A. Metallic Square Plate Buried Under a Flat Dielectric Surface

In this section, the PEC square plate is buried at a depth $d = \lambda_1$ from a dielectric flat surface which is illuminated by the tapered beam in the incidence direction $\hat{\mathbf{k}}_i(\theta_i = 0°, \phi_i = 0°)$ (normal incidence). In Fig. 4, we present the bistatic NRCS as a function of the scattering angle θ_s, for VV and HH polarizations. This figure indicates that PILE and PILE-ACA methods solving the rigorous PMCHW-EFIE formulation converge after $P_{\text{PILE}} = 2$ iterations with an error of 0.14%, whereas KA-PILE and KA-PILE-ACA methods solving the hybrid KA-EFIE formulation converge after $P_{\text{PILE}} = 2$ iterations with an error of 0.12%. This physically means that only two back-and-forth of the fields scattered from the flat surface to the buried PEC plate contribute to the NRCS. Given that the NRCS at the order $p = 0$ corresponds to that of the flat dielectric surface in the absence of the PEC square plate, we can deduce that the current-based KA correctly estimates the incident current densities.

Indeed, it can be shown from Fig. 4 that the results of PILE(0) are in a very good agreement with those of KA-PILE(0) in the specular lobe $\theta_s \in [-20°, 20°]$. For the other scattering direction, NRCS levels are very low ($\simeq 50$ dB below the maximum NRCS value). At the order $p = 2$, it can also be seen that the results of KA-PILE and KA-PILE-ACA are in a very good agreement with those of PILE and PILE-ACA around the specular direction in the region $\theta_s \in [-50°, 50°]$. By comparing the NRCS curves associated with the zeroth- and second-order, it can be observed that the total NRCS is mainly due to the dielectric flat surface contribution in the scattering directions defined by $\theta_s \in [-10°, 10°]$, whereas the PEC plate contribution to the NRCS is noticeable in the other scattering directions.

On the other hand, the curves show that the hybridization of the PILE method with the ACA (for hybrid and rigorous formulations) is very successful because it introduces no loss of accuracy on the NRCS. The PILE-ACA mean compression ratio of the coupling matrices is equal to 93.53% while the KA-PILE-ACA mean compression ratio of the coupling matrices is 88.19%. It should be noted that the mutual-reaction matrices (82.98%) are less compressed than the mutual-impedance matrices (93.66%). In other words, the effective ranks of the mutual-reaction matrices are higher than those of the mutual-impedance matrices. This may be due to the fact that these mutual-reaction matrices directly relate the current densities
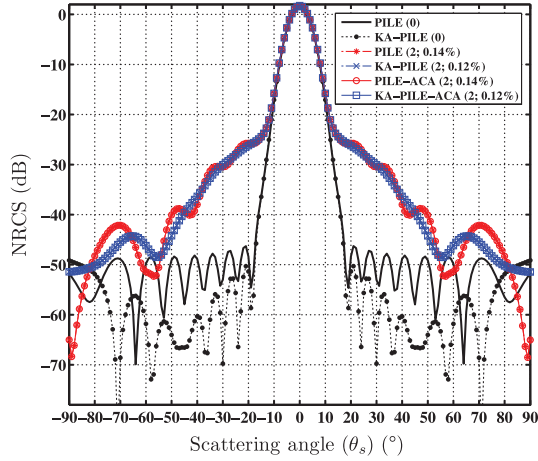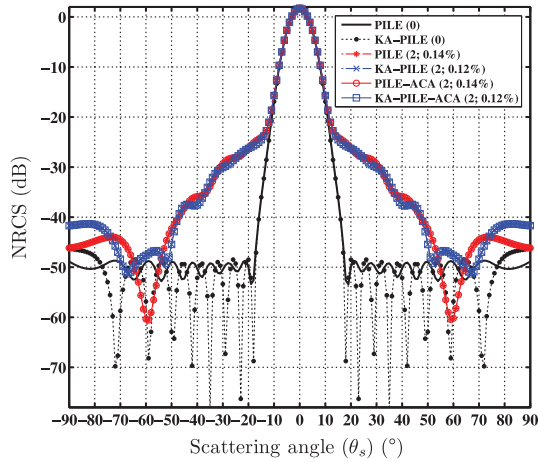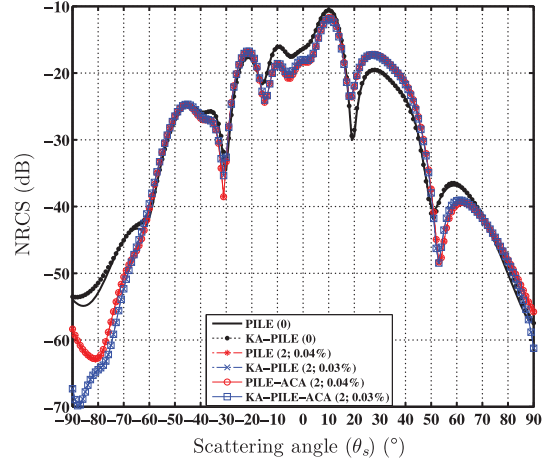
Fig. 4. Comparison between PMCHW-EFIE and KA-EFIE approaches on the copolarized bistatic NRCS of a PEC square plate buried at a depth $d = \lambda_1$ under a dielectric flat surface with respect to scattering angle θ_s for an incident wave frequency $f = 300$ MHz and direction $\hat{\mathbf{k}}_i(\theta_i = 0°, \phi_i = 0°)$. (a) VV-polarization. (b) HH-polarization.

Fig. 5. Comparison between PMCHW-EFIE and KA-EFIE approaches on the copolarized bistatic NRCS of a PEC square plate buried at a depth $d = \lambda_1$ under a dielectric rough surface ($\sigma_z = 0.2\lambda_1$, $l_c = 1.5\lambda_1$) with respect to scattering angle θ_s for an incident wave frequency $f = 300$ MHz and direction $\hat{\mathbf{k}}_i(\theta_i = 0°, \phi_i = 0°)$. (a) VV-polarization. (b) HH-polarization.

between the dielectric surface and the buried object (local informations such as Fresnel reflection coefficients are contained in these matrices).

A numerical experiment by decreasing the burial depth from $d = \lambda_1$ to $d = 0.5\lambda_1$ was made. It was found that the mean compression ratio of the mutual-impedance matrices becomes equal to 91.60% while that of the mutual-reaction matrices becomes 63.89% and the computational overhead of the ACA algorithm when applied to the mutual-reaction matrices becomes high. For this case, the mutual-reaction matrices are diagonally dominant, and hence, seldom rank-deficient. This leads us to conclude that the use of the ACA algorithm to compress the coupling matrices (particularly the mutual-reaction matrices) is only efficient for large burial depths.

B. Metallic Square Plate Buried Under a Rough Dielectric Surface: Impact of Incidence Angle on the Accuracy of the Hybrid KA-EFIE Approach

In this section, the dielectric flat surface is changed to be a dielectric rough surface obeying a Gaussian process with a
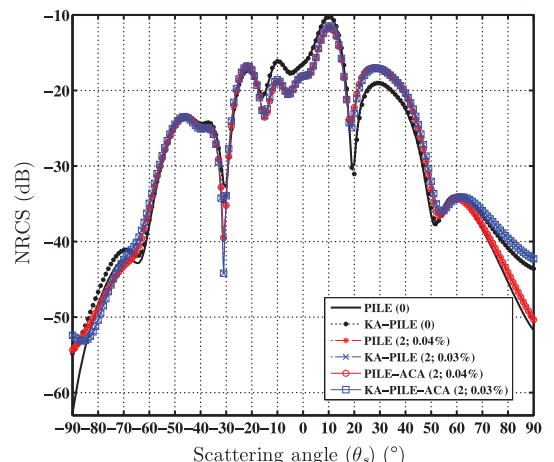
Gaussian height spectrum having a standard deviation height $\sigma_z = 0.2\lambda_1$ and a correlation length $l_c = l_{cx} = l_{cy} = 1.5\lambda_1$. The burial depth of the square PEC plate is $d = \lambda_1$. Two incidence directions are considered: $\hat{\mathbf{k}}_i(\theta_i = 0°, \phi_i = 0°)$ and $\hat{\mathbf{k}}_i(\theta_i = 20°, \phi_i = 0°)$. In Figs. 5 and 6, we present the bistatic copolarized NRCS as a function of the scattering angle θ_s for $\hat{\mathbf{k}}_i(\theta_i = 0°, \phi_i = 0°)$ and $\hat{\mathbf{k}}_i(\theta_i = 20°, \phi_i = 0°)$, respectively. The legends of these figures indicate that only two back-and-forth ($P_{\text{PILE}} = 2$) of the fields scattered from the rough surface to the buried PEC plate contribute to the NRCS. For both 0° and 20° incidences, the copolarized results of the hybrid formulation are in a very good concordance with those of the rigorous formulation, except for grazing scattering angles.

On the other hand, the hybridization of the PILE method with the ACA (for hybrid and rigorous formulations) is very successful and does not introduce a loss of accuracy on the NRCS. The PILE-ACA mean compression ratio of the coupling matrices is equal to 93.55% while the KA-PILE-ACA mean compression ratio of the coupling matrices is 88.58%. We found that the compression ratio of the coupling matrices does not vary with the incidence angle. However, we notice again that the
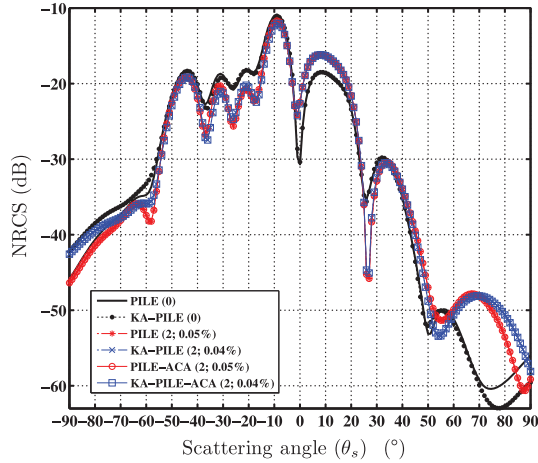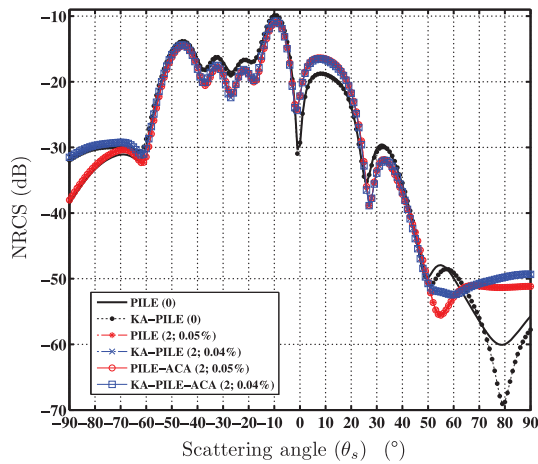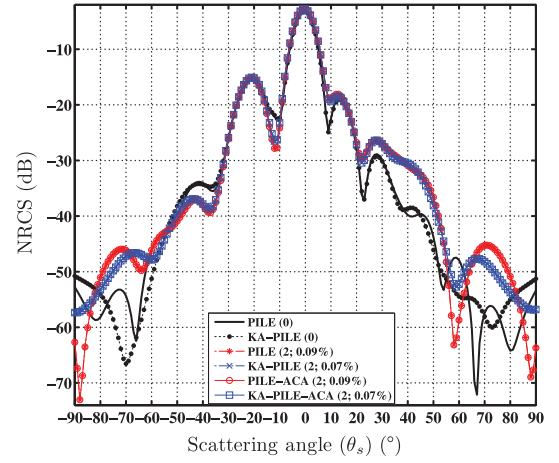
Fig. 6. Comparison between PMCHW-EFIE and KA-EFIE approaches on the copolarized bistatic NRCS of a PEC square plate buried at a depth $d = \lambda_1$ under a dielectric rough surface ($\sigma_z = 0.2\lambda_1$, $l_c = 1.5\lambda_1$) with respect to scattering angle θ_s for an incident wave frequency $f = 300$ MHz and direction $\hat{\mathbf{k}}_i(\theta_i = 20°, \phi_i = 0°)$. (a) VV-polarization. (b) HH-polarization.
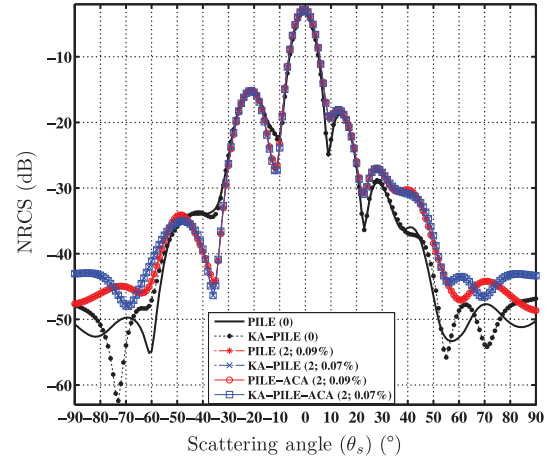

Fig. 7. Comparison between PMCHW-EFIE and KA-EFIE approaches on the copolarized bistatic NRCS of a PEC square plate buried at a depth $d = \lambda_1$ under a dielectric rough surface ($\sigma_z = 0.1\lambda_1$, $l_c = 1.5\lambda_1$) with respect to scattering angle θ_s for an incident wave frequency $f = 300$ MHz and direction $\hat{\mathbf{k}}_i(\theta_i = 0°, \phi_i = 0°)$. (a) VV-polarization. (b) HH-polarization.

mutual-reaction matrices (83.57%) are less compressed than the mutual-impedance matrices (93.60%) and they involve a high-computational overhead of the ACA algorithm. That is why, it may be wise to compress only the mutual-impedance matrices for short burial depths.

C. Metallic Square Plate Buried Under a Rough Dielectric Surface: Impact of the Surface Roughness on the Accuracy of the Hybrid KA-EFIE Approach

Now, two cases of surface roughness are considered: 1) a standard deviation height $\sigma_z = 0.1\lambda_1$ and a correlation length $l_c = l_{cx} = l_{cy} = 1.5\lambda_1$ and 2) a standard deviation height $\sigma_z = 0.2\lambda_1$ and a correlation length $l_c = l_{cx} = l_{cy} = 1\lambda_1$. The burial depth of the square PEC plate is $d = \lambda_1$. The rough surface is illuminated by the tapered beam in the incidence direction $\hat{\mathbf{k}}_i(\theta_i = 0°, \phi_i = 0°)$. For both cases, Figs. 7 and 8 show that the copolarized results obtained with the hybrid KA-EFIE approach agree with rigorous approach results, yet with visible discrepancies at grazing scattering angles. These discrepancies

are mainly due to the shadowing effects (not accounted for both in the calculation of the current densities) and multiple scattering interactions on the rough surface. By applying the bistatic average shadowing function given in [28] to the NRCS simulated by the hybrid KA-EFIE approach, it was observed that the discrepancies for $|\theta_s|$ close to 90° are decreased.

It is important to underline that the convergence order P_{PILE} is equal to 2 for both cases of surface roughness. As an auxiliary note, the PILE-ACA-based solver does not introduce a loss of accuracy on the NRCS compared to the conventional PILE-based solver. However, it is found that its effectiveness also depends on the roughness of the surface. In fact, for the first case, the KA-PILE-ACA mean compression ratios of the mutual-impedance and mutual-reaction matrices are equal to 93.60% and 84.77%, respectively, whereas they are equal to 93.51% and 79.66%, respectively, for the second case. The computational times required for solving the rigorous and hybrid formulations related to the first surface roughness case are specified in Table I, in order to illustrate the time reduction achieved by the hybrid approach.
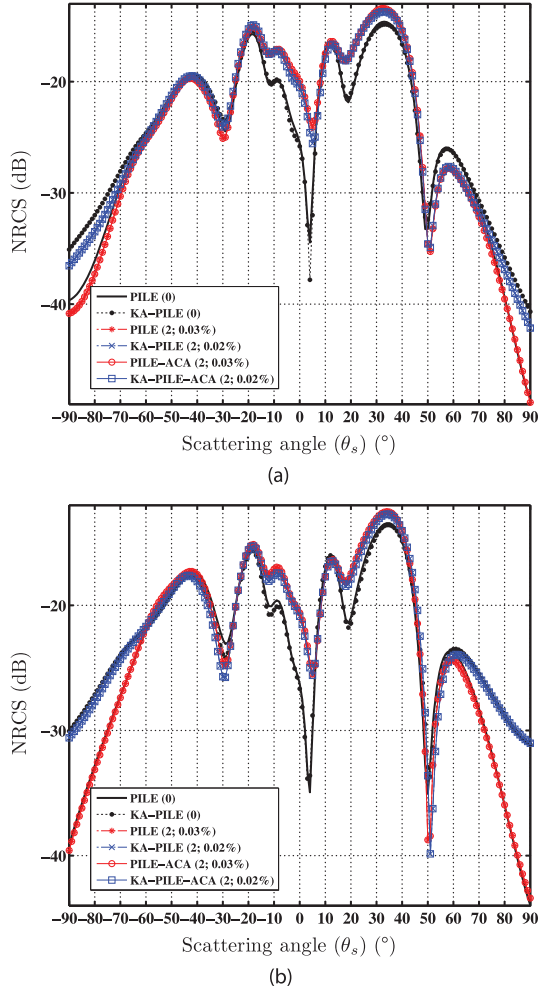
Fig. 8. Comparison between PMCHW-EFIE and KA-EFIE approaches on the copolarized bistatic NRCS of a PEC square plate buried at a depth $d = \lambda_1$ under a dielectric rough surface ($\sigma_z = 0.2\lambda_1$, $l_c = 1\lambda_1$) with respect to scattering angle θ_s for an incident wave frequency $f = 300$ MHz and direction $\hat{k}_i(\theta_i = 0°, \phi_i = 0°)$. (a) VV-polarization. (b) HH-polarization.

TABLE I
TOTAL SOLVING TIME RELATED TO THE SURFACE ROUGHNESS CASE
($\sigma_z = 0.1\lambda_1$ AND $l_c = l_{cx} = l_{cy} = 1.5\lambda_1$)

Solver \ Formulation	PMCHW-EFIE	KA-EFIE
PILE-based	6h : 26 min : 51s	0h : 05 min : 33s
PILE-ACA-based	6h : 04 min : 46s	0h : 05 min : 08s

In order to complete the numerical validation step, we present in Fig. 9, a comparison on the phase of copolarized scattered fields for the second surface roughness case. Fig. 9 shows that the phase of copolarized scattered fields obtained with the hybrid KA-EFIE approach also agrees with that simulated by the rigorous approach. Finally, it is important to mention that we did not present cross-polarized results because our hybrid KA-EFIE approach is unable to correctly predicting the depolarization coming from the surface roughness.

D. Metallic Sphere Buried Under a Rough Dielectric Surface

Let us now focus on a PEC sphere of radius $0.4\lambda_1$ buried at a depth $d = \lambda_1$ under a rough surface having a standard deviation
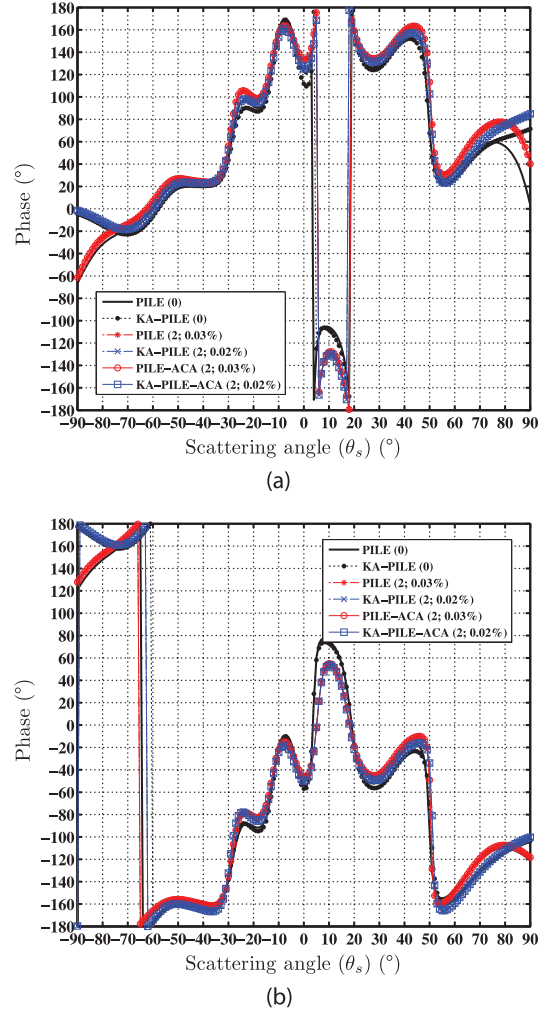

Fig. 9. Comparison between PMCHW-EFIE and KA-EFIE approaches on the phase of the electric field scattered from a PEC square plate buried at a depth $d = \lambda_1$ under a dielectric rough surface ($\sigma_z = 0.2\lambda_1$, $l_c = 1\lambda_1$) with respect to scattering angle θ_s for an incident wave frequency $f = 300$ MHz and direction $\hat{k}_i(\theta_i = 0°, \phi_i = 0°)$. (a) VV-polarization. (b) HH-polarization.

height $\sigma_z = 0.2\lambda_1$ and a correlation length $l_c = l_{cx} = l_{cy} = 1.5\lambda_1$. The rough surface is illuminated by the tapered beam at an incidence direction $\hat{k}_i(\theta_i = 0°, \phi_i = 0°)$.

In Fig. 10, we present the bistatic NRCS as a function of the scattering angle θ_s for VV and HH polarizations. This figure shows that the copolarized results obtained by the hybrid KA-EFIE approach agree with the rigorous approach results, except for grazing scattering angles where discrepancies can be observed. As mentioned earlier, these discrepancies are mainly due to the shadowing effects and multiple scattering interactions on the rough surface.

By comparing the PILE-ACA-based results with those of the PILE method, we can deduce that the ACA compression does not introduce a significant error on the NRCS. Furthermore, the KA-PILE-ACA mean compression ratios of the mutual-impedance and mutual-reaction matrices are equal to 94.33% and 88.17%, respectively. Finally, it can also be observed from Fig. 10 that the total response (sphere buried under the rough surface) and that of the rough surface only are almost comparable for a burial depth equals λ_1 in the scattering angular sector $|\theta_s| < 50°$.
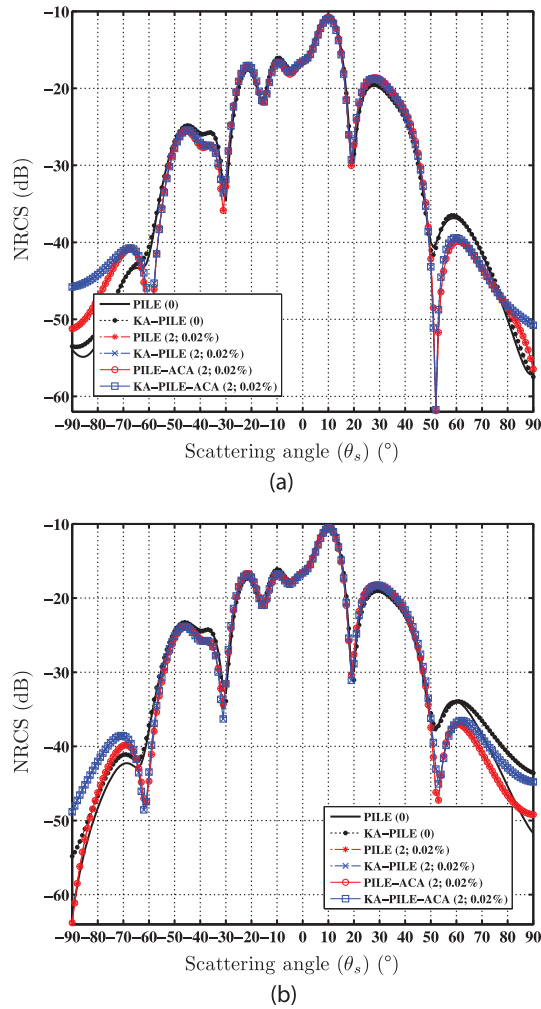
Fig. 10. Comparison between PMCHW-EFIE and KA-EFIE approaches on the copolarized bistatic NRCS of a PEC sphere buried at a depth $d = \lambda_1$ under a dielectric rough surface ($\sigma_z = 0.2\lambda_1$, $l_c = 1.5\lambda_1$) with respect to scattering angle θ_s for an incident wave frequency $f = 300$ MHz and direction $\hat{k}_i(\theta_i = 0°, \phi_i = 0°)$. (a) VV-polarization. (b) HH-polarization.

V. CONCLUSION

In this paper, a hybrid KA-EFIE approach has been presented for the evaluation of EM scattering from a PEC object buried beneath a dielectric rough surface. The KA-EFIE formulation is discretized using an MoM with RWG basis functions and it is then efficiently solved by the iterative PILE method combined with the algebraic ACA algorithm. This hybrid approach can deal with realistic scattering scenarios because it leads to a significant reduction in computation time and memory requirements in comparison to the rigorous PMCHW-EFIE formulation which requires solving a large MoM matrix equation. Some numerical results were presented to illustrate the accuracy, the versatility, and the usefulness of the PILE and PILE-ACA methods solving the KA-EFIE formulation. The ACA algorithm is used to accelerate the time-consuming coupling interaction between the rough surface and the buried object. Nevertheless, its efficiency depends on the burial depths as well as the surface roughness, especially when it is applied to the mutual-reaction matrices. Numerical simulations have

shown that a burial depth of one wavelength is enough for flat and slightly rough surfaces to obtain good compression ratios.

ACKNOWLEDGMENT

The authors would like to thank the anonymous reviewers for their constructive comments and suggestions that have contributed in improving the quality of this paper.

REFERENCES

[1] W. Chew *et al.*, *Integral Equation Methods for Electromagnetic and Elastic Waves*, USA: Morgan & Claypool Publishers, 2008.
[2] W. C. Gibson, *The Method of Moments in Electromagnetics*. Boca Raton, FL, USA: CRC Press, 2007.
[3] M. M. Ney, "Method of moments as applied to eelectromagnetic problems," *IEEE Trans. Microw. Theory Tech.*, vol. MTT-33, no. 10, pp. 972–980, Oct. 1985.
[4] C. Bourlier, N. Pinel, and G. Kubické, *Method of Moments for 2D Scattering Problems: Basic Concepts and Applications*. Hoboken, NJ, USA: Wiley, 2013.
[5] C. Bourlier, N. Pinel, and G. Kubické, "Propagation-inside-layer-expansion method combined with physical optics for scattering by coated cylinders, a rough layer, and an object below a rough surface," *J. Opt. Soc. Amer. A*, vol. 30, no. 9, pp. 1727–1737, 2013.
[6] C. Bourlier, G. Kubické, and N. Déchamps, "Fast method to compute scattering by a buried object under a randomly rough surface: PILE combined with FB-SA," *J. Opt. Soc. Amer. A*, vol. 25, no. 4, pp. 891–902, 2008.
[7] M. El-Shenawee, "Scattering from multiple objects buried beneath two-dimensional random rough surface using the steepest descent fast multipole method," *IEEE Trans. Antennas Propag.*, vol. 51, no. 4, pp. 802–809, Apr. 2003.
[8] M. El-Shenawee, "The multiple interaction model for nonshallow scatterers buried beneath 2-D random rough surfaces," *IEEE Trans. Geosci. Remote Sens.*, vol. 40, no. 4, pp. 982–987, Apr. 2002.
[9] M. El-Shenawee and C. M. Rappaport, "Monte Carlo simulations for clutter statistics in minefields: AP-mine-like-target buried near a dielectric object beneath 2-D random rough ground surfaces," *IEEE Trans. Geosci. Remote Sens.*, vol. 40, no. 6, pp. 1416–1426, Jun. 2002.
[10] M. El-Shenawee, C. Rappaport, and M. Silevitch, "Monte Carlo simulations of electromagnetic wave scattering from a random rough surface with three-dimensional penetrable buried object: Mine detection application using the steepest-descent fast multipole method," *J. Opt. Soc. Amer. A*, vol. 18, no. 12, pp. 3077–3084, 2001.
[11] G. Zhang, L. Tsang, and K. Pak, "Angular correlation function and scattering coefficient of electromagnetic waves scattered by a buried object under a two-dimensional rough surface," *J. Opt. Soc. Amer. A*, vol. 15, no. 12, pp. 2995–3002, 1998.
[12] S. M. Rao, D. Wilton, and A. W. Glisson, "Electromagnetic scattering by surfaces of arbitrary shape," *IEEE Trans. Antennas Propag.*, vol. 30, no. 3, pp. 409–418, May 1982.
[13] E. Ubeda and J. M. Rius, "MFIE MoM-formulation with curl-conforming basis functions and accurate kernel integration in the analysis of perfectly conducting sharp-edged objects," *Microw. Opt. Technol. Lett.*, vol. 44, no. 4, pp. 354–358, 2005.
[14] P. Yla-Oijala and M. Taskinen, "Calculation of CFIE impedance matrix elements with RWG and n×RWG functions," *IEEE Trans. Antennas Propag.*, vol. 51, no. 8, pp. 1837–1846, Aug. 2003.
[15] L. Medgyesi-Mitschang, J. Putnam, and M. Gedera, "Generalized method of moments for three-dimensional penetrable scatterers," *J. Opt. Soc. Amer. A*, vol. 11, no. 4, pp. 1383–1398, 1994.
[16] A. J. Poggio and E. K. Miller, *Integral Equation Solutions of Three-Dimensional Scattering Problems*, R. Mittra, Ed. New York, NY, USA: Pergamon, 1973.
[17] L. Zhou, L. Tsang, V. Jandhyala, Q. Li, and C. H. Chan, "Emissivity simulations in passive microwave remote sensing with 3-D numerical solutions of Maxwell equations," *IEEE Trans. Geosci. Remote Sens.*, vol. 42, no. 8, pp. 1739–1748, Aug. 2004.
[18] K. Pak, L. Tsang, and J. Johnson, "Numerical simulations and backscattering enhancement of electromagnetic waves from two-dimensional dielectric random rough surfaces with the sparse-matrix canonical grid method," *J. Opt. Soc. Amer. A*, vol. 14, no. 7, pp. 1515–1529, 1997.

[19] Q. Li, L. Tsang, K. S. Pak, and C. H. Chan, "Bistatic scattering and emissivities of random rough dielectric lossy surfaces with the physics-based two-grid method in conjunction with the sparse-matrix canonical grid method," *IEEE Trans. Antennas Propag.*, vol. 48, no. 1, pp. 1–11, Jan. 2000.

[20] M. El-Shenawee, C. Rappaport, E. L. Miller, and M. B. Silevitch, "Three-dimensional subsurface analysis of electromagnetic scattering from penetrable/PEC objects buried under rough surfaces: Use of the steepest descent fast multipole method," *IEEE Trans. Geosci. Remote Sens.*, vol. 39, no. 6, pp. 1174–1182, Jun. 2001.

[21] L. Tsang and J. A. Kong, *Scattering of Electromagnetic Waves, Advanced Topics*, vol. 26. Hoboken, NJ, USA: Wiley, 2004.

[22] J. A. Kong, *Electromagnetic Wave Theory*, Cambridge, MA, USA: EMW Publishing, 2005.

[23] N. Déchamps, N. Beaucoudrey, C. Bourlier, and T. Serge, "Fast numerical method for electromagnetic scattering by rough layered interfaces: Propagation-inside-layer-expansion method," *J. Opt. Soc. Amer. A*, vol. 23, no. 2, pp. 359–369, 2006.

[24] K. Zhao, M. N. Vouvakis, and J.-F. Lee, "The adaptive cross approximation algorithm for accelerated method of moments computations of EMC problems," *IEEE Trans. Electromagn. Compat.*, vol. 47, no. 4, pp. 763–773, Nov. 2005.

[25] H. Braunisch *et al.*, "Tapered wave with dominant polarization state for all angles of incidence," *IEEE Trans. Antennas Propag.*, vol. 48, no. 7, pp. 1086–1096, Jul. 2000.

[26] U. Jakobus and F. M. Landstorfer, "Improved PO-MM hybrid formulation for scattering from three-dimensional perfectly conducting bodies of arbitrary shape," *IEEE Trans. Antennas Propag.*, vol. 43, no. 2, pp. 162–169, Feb. 1995.

[27] S. Kurz, O. Rain, and S. Rjasanow, "The adaptive cross-approximation technique for the 3D boundary-element method," *IEEE Trans. Magn.*, vol. 38, no. 2, pp. 421–424, Mar. 2002.

[28] N. Pinel and C. Boulier, *Electromagnetic Wave Scattering From Random Rough Surfaces: Asymptotic Models*. Hoboken, NJ, USA: Wiley, 2013.

Sami Bellez was born in Djerba, Tunisia, in 1981. He received the Ph.D. degree in electronics and electrical engineering from the University of Paris VI, Paris, France, in 2010.

He has been with the Laboratory of Signal and System (L2S), Supèlec, Gif-sur-Yvette, France, working in the field of EM scattering by forests. Then, he joined with the Laboratory of Electronic and Electromagnetism (L2E), the University of Paris VI for a work on bistatic synthetic aperture radar (SAR) imagery. Between 2011 and 2013, he was a Postdoctoral Research Fellow (financed by the French Space Agency CNES) with the Institute of Electronics and Telecommunications of Rennes, France (IETR) Laboratory, Rennes, France. Currently, he is a Research Scientist with the IETR, Polytech'Nantes, Nantes. His research interests include EM wave propagation and scattering in random media and from rough surfaces, microwave remote sensing, computational EMs and SAR imaging techniques (interferometry and tomography).

Christophe Bourlier was born in La Flèche, France, on July 6, 1971. He received the M.S. degree in electronics from the University of Rennes, Rennes, France, in 1995, and the Ph.D. degree in electronics and electrical engineering from the Systme Électronique et Informatique (SEI) Laboratory, Nantes, France, in 1999.

He is now with the Institute of Electronics and Telecommunications of Rennes, France (IETR) Laboratory, Nantes, at Polytech'Nantes (University of Nantes, France). He is a Researcher with the National Center for Scientific Research working on EM wave scattering from rough surfaces (ocean-like surfaces) and objects for microwaves and infrared remote sensing applications and radar signatures.

Gildas Kubické was born in Longjumeau, France, in September 1982. He received the Engineering and M.S. degrees in electronics and electrical engineering from Polytech'Nantes, Nantes, France, in 2005, and the Ph.D. degree in electronics and electrical engineering from the University of Nantes, Nantes, France, in 2008.

Then he was a Research Engineer with the Institut de Recherche en Electrotechnique et Electronique de Nantes Atlantique (IREENA) Laboratory, Nantes, France. In 2010, he joined with the Direction Générale de l'Armement (DGA), French Ministry of Defense, where he works as an expert in the field of radar signatures and EM stealth. He is in charge of the "Expertise in electroMagnetism and Computation" (EMC) Laboratory. His research interests include EM scattering and diffraction, radar cross-section (RCS) measurement and modeling, asymptotic high-frequency methods, and fast numerical methods.